ISSN 2616-5767 Vol.7, Issue 5: 98-110, DOI: 10.25236/AJETS.2024.070513

Design of Locking Mechanism and Locking Performance Analysis for Folding Wing

Haizhong Huang[1,a], Chenglong Zhang[1,b,*], Shunbo Yang[1,c], Cheng Huang[1,d], Chongtian Zhang[1,e]

[1]Department of Mechanical Engineering, Harbin Institute of Technology at Weihai, Weihai, 264209, China
[a]hu_anghaihzong_go@126.com, [b]jobhitwhzcl@126.com, [c]yang0913103@163.com,
[d]2021212194@stu.hit.edu.cn, [e]18526133382@163.com
[*]Corresponding author

Abstract: *To address the issue of insufficient locking performance of the spring-cone pin structure for the folding wing control surface, a self-locking square inclined-plane pin structure was designed. Physical testing showed that the use of square inclined-plane pins in the locking mechanism can achieve repeated and reliable locking of the control surface. A theoretical predictive model for the static stiffness and frequency characteristics of the folding wing locking state was established. Through simulation and experimental testing, the prediction error of the theoretical model was below 15%.*

Keywords: *folding rudders wings, locking mechanism, static stiffness, frequency characteristics*

1. Introduction

The folded rudder wing can meet the transverse dimension constraints of the launch platform on the wing/rudder, meet the different requirements of different flight sections in the flight profile for control capabilities, improve the loading capacity of the platform, and facilitate ground service processing, which is of great significance in the application of high-speed aircraft. The current research on folding wing dynamics mainly focuses on the dynamic analysis, aerodynamic performance analysis and experimental testing of the unfolding process. Robert Kroyer [1] carried out a detailed analysis of the wing mechanism. Andrzej T, Tomasz G G. [2] proposed to optimize the position design of the hinge system of the folding wing. J. I. Henry et al. [3] introduced the development and test of a prototype flexible foldable wing micro-aerial vehicle (MAV). Dowell EH. And Tang D.[4] discussed the latest progress of nonlinear aeroelasticity and unsteady aerodynamics of airfoil. Hu, Wei Yang et al. [5, 6] studied the aeroelastic characteristics of folded wing during deformation. Zhang, Wei et al. [7] proposed a parametric aeroelastic analysis method to study the aeroelastic stability of folded wings. S. Bograd et al. [8] outlined different approaches to the dynamics of mechanical joints in modeling assembly structures, including joint characteristics, joint model types, and friction models, and provided detailed introductions to three joint modeling methods based on the finite element method, as well as practical application cases and tutorial examples. Santos et al. [9] studied the effects of geometric and inertial parameters on the mass of variable span wing structure. Abdelkefi A. et al. [10] proposed a nonlinear analysis of a two-degree-of-freedom aeroelastic system to identify the freeplay nonlinearity in the pitch degree of freedom and its impact on the system's bifurcation characteristics. M. V. Yarygina and Yu. I. Popov [11] determined the factors affecting the position of folding axis and the increase of the mass of folded wing. Dae-Kwan Kim et al. [12] established a nonlinear dynamic model of the deployable missile control wing, and Jae-Sung Bae et al studied the nonlinear aeroelastic characteristics of the controllably deployable folding wing of the missile. Jae-Sung Bae et al. [13] presented a nonlinear aeroelastic analysis of the dynamics of a deployable missile control fin, which elucidates the significant influence of the fin's nonlinear aerodynamic characteristics and structural elasticity on its dynamic response, providing a theoretical basis for the design optimization of such deployable control surfaces.

The above studies have been relatively comprehensive in the study of the folding rudder wing, but there are few studies on the in-place locking mechanism and the inherent characteristics of the folding wing structure. A typical folding wing consists of fixed wing surfaces, movable wing surfaces, actuation mechanisms, and locking mechanisms. The in-place locking mechanism is a key component determining whether the folded wing surfaces can be reliably locked in position. The in-place locking mechanism is

ISSN 2616-5767 Vol.7, Issue 5: 98-110, DOI: 10.25236/AJETS.2024.070513

usually a pin structure, such as a pyrotechnic pyro-drive pin or a spring-driven spring pin locking mechanism. The locking process of the pyrotechnic pyro-drive pin requires time sequence control, making its principle complex, reliability poor, and cost high, hence the more common application of spring pin locking mechanisms.

The post-locking performance of folding rudders/wings is the current research focus. In the aforementioned studies, the designed locking pins are all cylindrical or conical pin structures. In practical testing and application, they often experience gaps on the mating surfaces due to bearing high loads, leading to sticking or locking failure, making it difficult to ensure the locking performance of the control surfaces. Additionally, current analyses of the locking state performance of folding rudders/wings are mostly based on simulation analyses, with long research and modeling cycles. Therefore, this paper designs a square inclined-plane locking structure and conducts theoretical modeling analysis of the static stiffness and dynamic characteristics performance of the folding rudder locking state, providing a theoretical prediction method.

2. Locking Mechanism Design

2.1. Mechanism composition

The general structure of a folding rudder is shown in Figure 1, typically locked in place by a spring-loaded locking pin mechanism. When the rudder is fully deployed, the locking pin extends to secure it in place. Commonly used locking pins, such as cylindrical pins or conical pins, are chosen for ease of manufacturing and assembly. However, it is often challenging to ensure the reliable implementation of the locking function during practical testing.

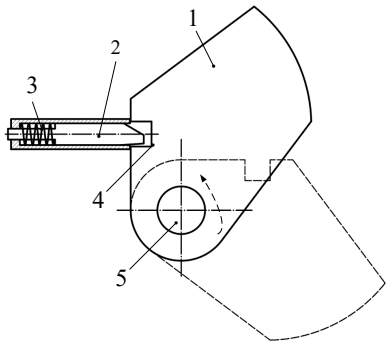

1-rudder, 2-locking pin, 3-compressed spring, 4-knock hole, 5-spiale

Figure 1: Folding rudder structure schematic

This paper introduces a spring-loaded locking mechanism based on a square pin and a self-locking inclined surface at the bottom, as illustrated in Figure 2. The structure mainly consists of a locking pin, a compression spring, a locking sleeve, and a positioning pin.

The locking pin design in conjunction with the rudder structure is depicted in Figure 3. The upper surface of the locking pin is designed with a large-angle inclined plane to ensure that before the folding rudder is fully unfolded, the pin retracts upon impact with the fixed rudder surface. The lower surface of the locking pin is designed with a small-angle self-locking inclined surface, which, in conjunction with the inclined plane, reduces the locking gap and ensures reliable locking.

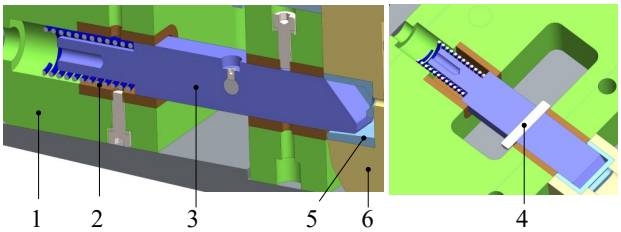

1. dynamic rudder surface 2. compressed spring 3. lock pin 4. limit pin 5. lock sleeve 6.fixed rudder surface

Figure 2: Spring pin locking mechanism diagram

ISSN 2616-5767 Vol.7, Issue 5: 98-110, DOI: 10.25236/AJETS.2024.070513

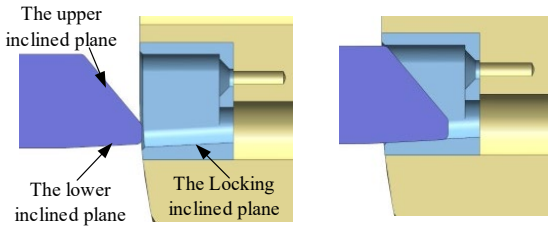

Figure 3: Locking structure design of locking pin

2.2. Working process of spring locking mechanism

During the unfolding process of the folding rudder, the locking pin, under the combined action of a compression spring and a limiting screw, remains in an extended state. Starting from the illustrated position, the inclined surface on the locking pin comes into contact with the fixed rudder surface, causing it to be compressed, as shown in Figure 4. As the rudder continues to unfold, the locking pin, compressed by the fixed rudder surface, maintains its compression and undergoes relative sliding with it. When the flap fully opens, the locking pin aligns with the hole on the fixed rudder surface. With the action of the spring force, the locking pin accurately inserts into the hole, completing the locking of the wing surface. At this point, the spring is still in a compressed state, leaving a portion of the spring force to prevent the locking pin from vibrating and rebounding.

In the locked state, the lower inclined surface of the locking pin cooperates to allow for a small upward displacement of the moving rudder surface, ensuring a tight fit between the contact surfaces of the moving rudder surface and the fixed rudder surface, thereby achieving reliable locking.

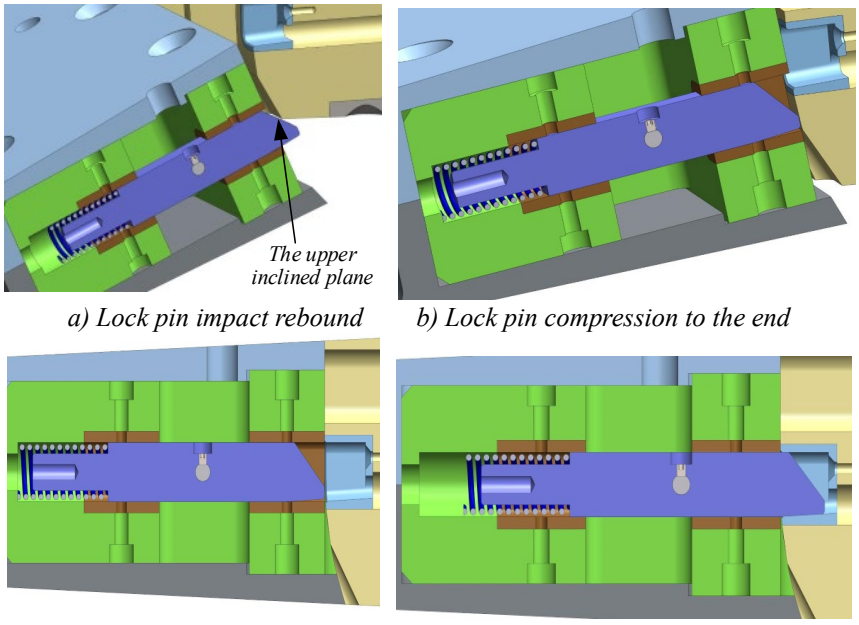

a) Lock pin impact rebound *b) Lock pin compression to the end*

c) Rudder spread in place *d) The locking pin ejects the lock*

Figure 4: Working process of spring locking mechanism

3. Theoretical Modeling

3.1. Static stiffness analysis

According to the design requirements, the normal equivalent concentrated force on the rudder surface should not be less than 60KN, corresponding to a moment of 16.5KNm. With a safety factor of 1.4, we can analyze the point of application of the equivalent concentrated force based on the geometric parameters of the rudder surface. When the rudder surface is subjected to an equivalent concentrated force, it undergoes both transverse bending and torsion relative to the rudder axis simultaneously. Assuming the rudder surface is an ideal linear elastic body, meaning the material is uniform and isotropic, and it follows Hooke's Law within the elastic range. According to the Castigliano's second theorem, the

ISSN 2616-5767 Vol.7, Issue 5: 98-110, DOI: 10.25236/AJETS.2024.070513

linear displacement of the rudder surface, treated as a cantilever beam under the action of normal equivalent concentrated force, is described as in Equation (1). Based on the definition of stiffness, the force causing unit deformation is considered as the static stiffness index of the mechanism.

$$\frac{\partial U}{\partial P_i} = \delta_i \tag{1}$$

Where, U represents the deformation energy of the cantilever beam rudder surface; P_i represents force of the load acting on the rudder surface; δ_i represents displacement of the structure in the P_i direction.

3.1.1. Torsional stiffness analysis

Under the action of a concentrated force at the trailing edge, the torsional deformation energy of the rudder surface is given by:

$$U = \int_0^L \frac{M_n{}^2(y)}{2GJ_p} dy \tag{2}$$

Where, J_p is the polar moment of inertia of the torsional section.

The equivalent torsional moment is:

$$M_n(y) = P \cdot d' \tag{3}$$

The deformation angle can be calculated as:

$$\theta = \int_0^L \frac{M_n(y)}{GJ_p} dy \tag{4}$$

Resulting in the torsional equivalent stiffness:

$$K_n = \frac{M_n}{\theta} \tag{5}$$

3.1.2. Bending stiffness analysis

By employing deflection analysis method and considering the rudder surface is subjected to bending concurrently with lateral shear forces, the bending deformation energy is given by:

$$U = \int_0^L K \frac{Q^2(y)}{2GA} dy + \int_0^L \frac{M^2(y)}{2EI} dy \tag{6}$$

Where A and I are the shear section area and bending section moment of inertia, respectively.

According to the principles of material mechanics, the torsional moment, shear force, and bending moment acting on the rudder surface can be represented as:

$$\begin{cases} Q(y) = P = M / L \\ M(y) = P \cdot (L - y) \end{cases} \tag{7}$$

Thus, the displacement at the point of action on the rudder surface is:

$$\delta = \int_0^L K \frac{P'}{GA} dy + \int_0^L \frac{P \cdot (L-d)}{EI_1} dy + \int_d^L \frac{P \cdot (d-y)^2}{EI_2} dy \tag{8}$$

where, M_n is the equivalent torsional moment acting on the rudder surface, K is the uniformly distributed shear stress coefficient, taken as 1.15, A is the shear section area, δ is the total displacement at the point of equivalent force concentration.

By substituting the parameters of the model into the above expressions, the deflection at the trailing edge can be obtained.

ISSN 2616-5767 Vol.7, Issue 5: 98-110, DOI: 10.25236/AJETS.2024.070513

$$\delta = \int_0^L \left(\frac{Pd^2}{0.325k_1bh^3G} + K\frac{P}{k_2bhG} + \frac{12P(L-y)^2}{k_1bh^3E} \right) dy \tag{9}$$

3.1.3. Analysis of Contact Deformation between Lock Pins and Pivot Shafts

The entire folding rudder can be divided into four parts, namely the movable rudder surface, fixed rudder surface, lock pins, and pivot shafts. As shown in Figure 5, through stress analysis, it can be inferred that when the tip cord of the movable rudder surface is loaded, the lock pins will be subjected to shear forces from the fixed rudder surface and movable rudder surface, resulting in contact deformation on the upper and lower surfaces under small displacement conditions. Similarly, the pivot shaft of the movable rudder surface is also affected by the forces from the fixed rudder surface and movable rudder surface, leading to contact deformation between the movable rudder surface and the pivot shaft, as well as between the fixed rudder surface and the pivot shaft.

By simplifying the contact at the lock pin location as cylindrical plane contact and cylindrical concave surface contact, according to the Hertz contact theory, the formula for calculating contact deformation can be obtained (10).

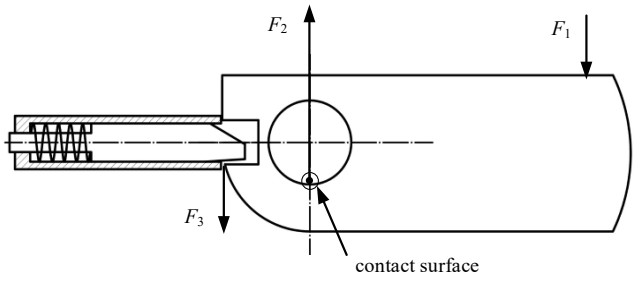

Figure 5: Analysis of the force on the rudder surface

$$\begin{cases} \delta_1 = 1.159\dfrac{F}{lE}(0.41 + \ln\dfrac{4R}{b_1}) \\ \delta_2 = 1.82\dfrac{F}{lE}(1 - \ln b_2) \end{cases} \tag{10}$$

Therein

$$\begin{cases} b_1 = 1.522\sqrt{\dfrac{FR}{lE}} \\ b_2 = 1.522\sqrt{\dfrac{F}{lE}\dfrac{R_1R_2}{R_2 - R_1}} \end{cases}$$

where δ_1 and δ_2 are deformations at the cylindrical surface of the locking pin and the cylindrical concave surface of the shaft, b_1, b_2 are the contact surface dimensions at the locking pin and shaft respectively, F is the force at the contact point; l is the length of the line contact, E is the elastic modulus of the contact material, R is the radius of the contact cylindrical surface at the locking pin, R_1、$R_2$are respective radius of the shaft and the shaft sleeve, obtained from measurements.

3.1.4. Overall Stiffness Analysis

Based on the aforementioned torsion and stiffness analysis, when the rudder surface is under load, torsion and bending usually occur simultaneously, and the combined effects of both are coupled. Taking into account the contact stiffness of the lock pins and pivot shafts mentioned earlier, the displacement at the load point on the rudder surface is considered as the total deformation, and it is used as the evaluation index for the overall static stiffness of the mechanism.

$$K = \frac{P}{\delta_m} \tag{11}$$

ISSN 2616-5767 Vol.7, Issue 5: 98-110, DOI: 10.25236/AJETS.2024.070513

3.2. Frequency characteristic analysis

3.2.1. Torsional Frequency Analysis

Assuming that the folding rudder is not subject to external forces, the dynamic differential equation of the mechanical system can be expressed as:

$$J\ddot{\theta} + c\dot{\theta} + K\theta = 0 \tag{12}$$

Where J represents the rotational inertia of the rudder surface about the pivot axis, K represents the bending stiffness of the rudder surface, c represents structural damping.

Neglecting structural damping and decomposing the angular displacement into a simple harmonic motion form, we have:

$$J\ddot{\theta} + K\theta = 0 \tag{13}$$

$$\theta = A\sin(\omega t + \varphi) \tag{14}$$

where A is the non-zero amplitude; w is the angular frequency, t is the time, φ is the initial phase angle. By combining the above two equations, we have:

$$\left(K - \omega^2 J\right) A = 0 \tag{15}$$

Thus, the natural frequency is obtained as:

$$\omega = \sqrt{\frac{K}{J}} \tag{16}$$

According to the previous torsional stiffness analysis and frequency definition, the torsional frequency of the mechanism is approximately 256Hz.

3.2.2. Bending Frequency Analysis

Considering the locked state of the rudder surface as an Euler-Bernoulli beam, neglecting shear deformation and the effect of cross-sectional rotation about the neutral axis on bending, according to the Rayleigh-Ritz method, considering the complexity of the modal functions for the cantilever beam with identical cross-sections, power functions are chosen as the basis functions. To ensure the accuracy of estimating the second-order modal frequency, three power functions are selected as a combination:

$$\phi_1(x) = \left(\frac{x}{l}\right)^2, \quad \phi_2(x) = \left(\frac{x}{l}\right)^3, \quad \phi_3(x) = \left(\frac{x}{l}\right)^4 \tag{17}$$

Obviously, the fixed end boundary conditions are satisfied. The Rayleigh-Ritz equivalent stiffness matrix is defined as:

$$\tilde{M} = (m_{ij}), \quad \tilde{K} = (k_{ij})$$
$$\left.\begin{aligned} m_{ij} = m_{ji} = \int_0^l \rho S(x)\phi_i(x)\phi_j(x)dx \\ k_{ij} = k_{ji} = \int_0^l EI(x)\phi_i''(x)\phi_j''(x)dx \end{aligned}\right\} \quad (i,\ j = 1,2,\cdots,n) \tag{18}$$

Where S is the equivalent cross-sectional area, and I is the equivalent bending moment of inertia of the cross-section. The characteristic equation:

$$(\tilde{K} - \tilde{\omega}^2\tilde{M})\boldsymbol{a} = 0 \tag{19}$$

Yields the eigenvectors and eigenvalues:

$$V_{\max} = \frac{1}{2}\int_0^l EI(x)[f''(x)]^2 dx = \frac{1}{2}\int_0^l \frac{M^2(x)}{EI(x)}dx \tag{20}$$

The equivalent bending stiffness of the rudder surface is:

ISSN 2616-5767 Vol.7, Issue 5: 98-110, DOI: 10.25236/AJETS.2024.070513

$$k = \int_0^l \frac{M^2(x)}{EI(x)} dx \tag{21}$$

Solving for the approximate values of the modal functions:

$$\phi_1(x) = 0.7049\left(\frac{x}{l}\right)^2 + 0.5501\left(\frac{x}{l}\right)^3 + 0.4478\left(\frac{x}{l}\right)^4 \tag{22}$$

$$\phi_2(x) = -0.2952\left(\frac{x}{l}\right)^2 - 0.6164\left(\frac{x}{l}\right)^3 - 0.7300\left(\frac{x}{l}\right)^4 \tag{23}$$

Approximately, the first-order bending frequency is estimated at 132Hz.

4. Simulation analysis verification

4.1. Static stiffness simulation

When not considering structural clearances and wire contact deformation, using the above calculation method, the theoretical analysis shows that the total displacement at the sagging point under the action of the equivalent concentrated force is approximately 32.7 mm. While the simulation analysis shows a displacement of 28.55 mm as shown in Figure 6, with an error percentage of about 12.8%.

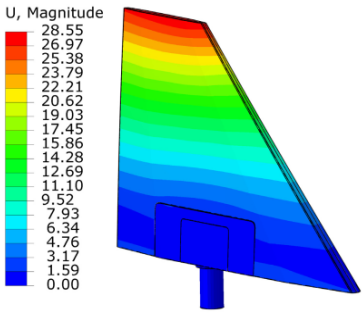

Figure 6: Static stiffness simulation analysis results

4.2. Modal simulation analysis

Model processing and analysis were conducted using ABAQUS, and the front three modal frequencies of the mechanism were obtained as shown in Figure 7. Comparing the simulation results with the aforementioned theoretical analysis, it can be observed that the mechanism's first-order modal frequency is close to the theoretical analysis result, with the maximum amplitude position consistent with the theoretical analysis result. The second-order modal frequency and third-order torsional mode are also relatively close to the theoretical calculation results, indicating to a certain extent the correctness of the theoretical model.

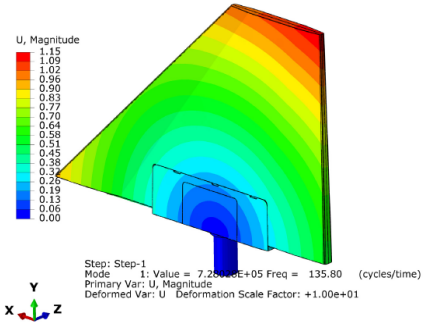

a) First Order Modal: 135.8Hz

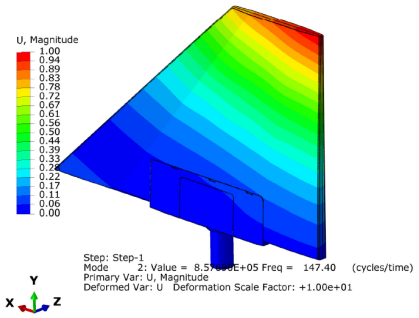

b) Second Order Modal: 147.4Hz

ISSN 2616-5767 Vol.7, Issue 5: 98-110, DOI: 10.25236/AJETS.2024.070513

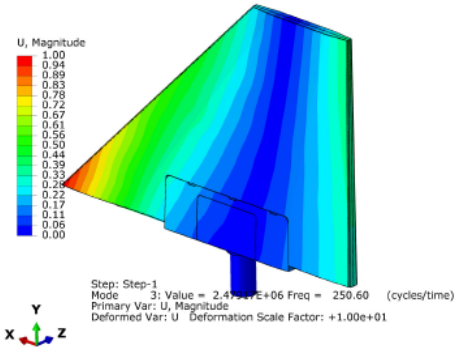

c) Third Order Modal: 250.6Hz

Figure 7: Results of modal simulation analysis of rudder surface

5. Test verification

5.1. Prototyping testing

The prototype of the folding rudder based on the previous locking mechanism, as shown in Figure 8-a). Principle the structure and material selection of the prototype are consistent with the design model, but the part of the rudder plane fixed by the chord is vertically installed to the profile frame, instead of the rudder shaft. Its movement process is shown in Figure 8. After it is deployed in place, effective locking can be achieved, and each separation surface is in good contact with no obvious gap.

a) Start to unfold

b) Lock pin compression in expansion

c) Near complete development

d) Unfold into position and lock

Figure 8: Folding rudder deployment locking process test

5.2. Static stiffness performance test

To test the static stiffness performance of the prototype according to the principles and to validate the theoretical prediction model of the static stiffness of the folding rudder, a test structure model for the static stiffness of the folding rudder prototype is designed as shown in Figure 9. To ensure that the rudder surface is securely fixed to the base platform and to simulate the real fixed state, thickened fixing fixtures are used to connect and lock the simulated rudder axis on the rudder surface. A concentrated load is applied to the rudder chord at the tip, the load magnitude is monitored by a force sensor, and the

ISSN 2616-5767 Vol.7, Issue 5: 98-110, DOI: 10.25236/AJETS.2024.070513

displacement of the load application point is measured using a dial gauge. Real-time recording of the data on the load and displacement at the application point is conducted to complete the test validation.

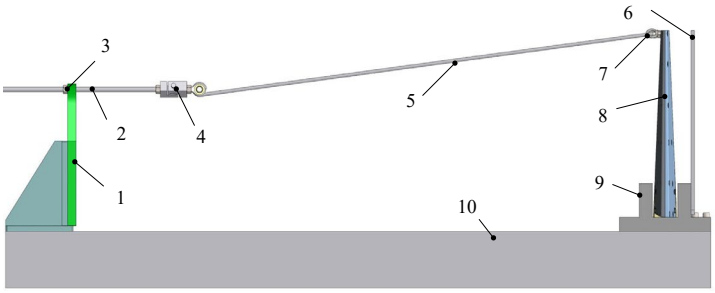

1. Loading plate 2. Loading screw 3. Loading nut 4. force sensor 5. Rope 6. Displacement datum plate 7. lifting nut 8. rudder 9. fixed station 10. Cast iron platform

Figure 9: Static stiffness performance test scheme

The installation of the dial gauge for displacement measurement is shown in Figure 10. The pointer contacts the line of action of the tension rope to monitor the displacement of the point of action of the resultant force (also referred to as the theoretical point of application of force).

Figure 10: Displacement measuring tool for the rudder tip chord

The prototype of the folding rudder principle is influenced by factors such as design tolerances and processing and assembly errors, resulting in actual structural clearances. These clearances exist in the mating installation surfaces of various components, with the main sources of influence on structural stiffness performance being the clearances between the locking pin and its sleeve and between the pivot shaft and its coaxial sleeve, as shown in Figure 11. After measuring the dimensions of the processed parts, the clearances between these components are found to be 0.03 mm and 0.04 mm, respectively. Therefore, when the rudder surface is subjected to loading, the elimination of structural clearances will cause additional displacements.

Figure 11: Measured dimensions of the matching surface of lock pin sleeve and lock pin

By combining measured processing clearances of workpieces and the stiffness of the torsion bar assembly to modify the theoretical model, the tension load and deflection data of the rudder surface obtained through theoretical calculations and measurements were processed using data analysis software to fit the deformation curve under load, as shown in Figure 12. The fitted curve indicates a good linear relationship between the deformation at the rudder surface and the load.

ISSN 2616-5767 Vol.7, Issue 5: 98-110, DOI: 10.25236/AJETS.2024.070513

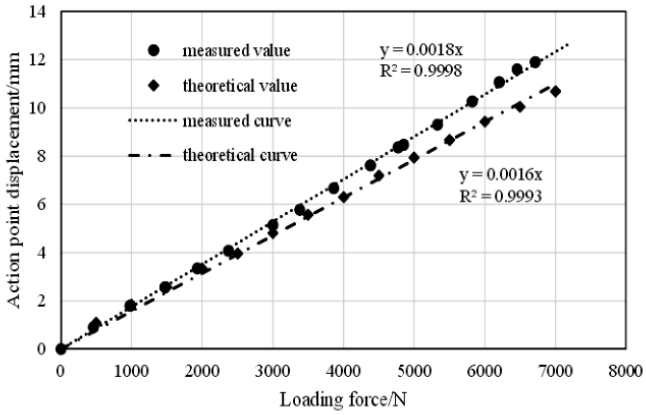

Figure 12: Curve of static stiffness of rudder surface

According to the theoretical calculation model, when a load of 6.7N is applied at the point of action, the theoretical deformation displacement at that point is approximately 10.3mm. Compared with the measured result, the error is about 14.4%. This discrepancy indicates the correctness of the theoretical model to a certain extent.

Both the measured curve and the theoretical analysis curve exhibit good linearity. The slope of the curve represents the flexibility of the structural mechanism, with the reciprocal representing the stiffness of the structure. The measured average stiffness is approximately 5.55e5N/m, while the theoretical average stiffness is 6.25e5N/m, resulting in a relative error of about 12.5%.

Analyzing the deformation displacements under the equivalent concentrated force (approximately 26KN) from the measured fitted curve, theoretical predictive curve, and theoretical calculation model yields values of 46.9mm, 41.7mm, and 38.3mm, respectively. The maximum relative error is about 18.4%. However, further measurements are still required for the deformation under this force.

Further analysis reveals that the stiffness obtained from the theoretical model is significantly greater than the actual tested stiffness. This is mainly due to the complexity of the actual mechanism, potential misalignment and deformation of some components during loading, and unpredictable nonlinear variations caused by structural clearances. The theoretical model only considers processing errors, clearances, and component contact stiffness, and simplifies the rudder surface structure, leading to weaker measured structural stiffness.

In conclusion, the experimental results indicate that the static stiffness theoretical model based on the folding rudder principle can accurately describe the prototype.

5.3. Rudder frequency test

To test the frequency characteristics of the prototype based on the principle and validate the theoretical prediction model of the folding rudder's frequency characteristics, a folding rudder frequency testing fixture was designed as shown in Figure 13. Dynamic signal analyzers were utilized with the impact method for testing, arranging signal measurement points at positions 1 and 2 on the rudder surface where the maximum amplitude occurs.

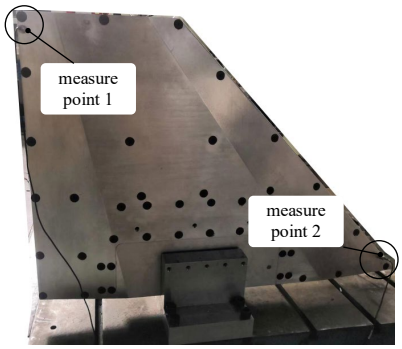

Figure 13: Rudder frequency test kit

ISSN 2616-5767 Vol.7, Issue 5: 98-110, DOI: 10.25236/AJETS.2024.070513

Frequency testing was conducted using both near-point impact and random impact methods. Frequency response curves for measurement point 1 are shown in Figures 14 and 15, while the corresponding frequency response curves for measurement point 2 are shown in Figures 16 and 17.

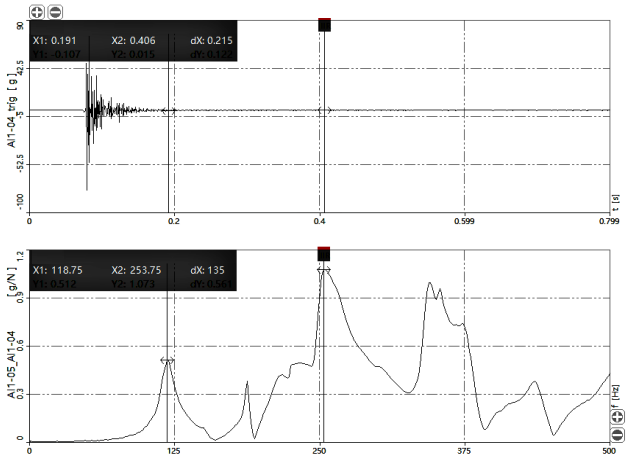

Figure 14: Tapping frequency response curve near measuring point 1

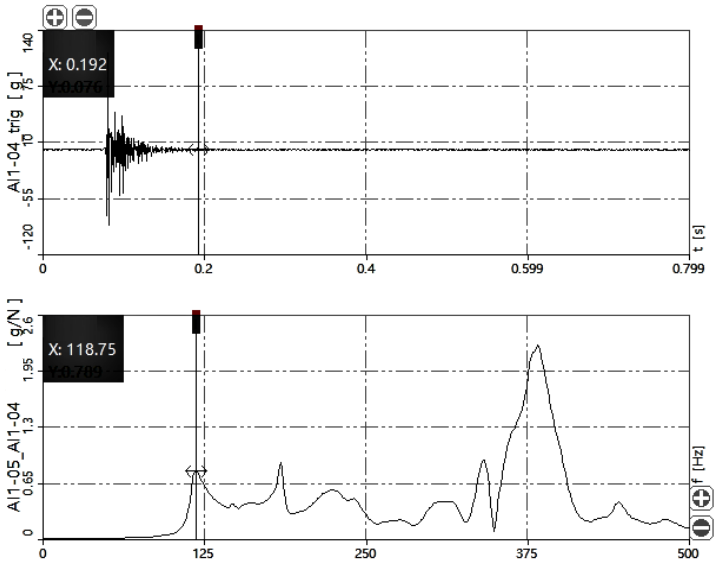

Figure 15: Frequency response curve of point 1 by randomly knock on the whole rudder plane

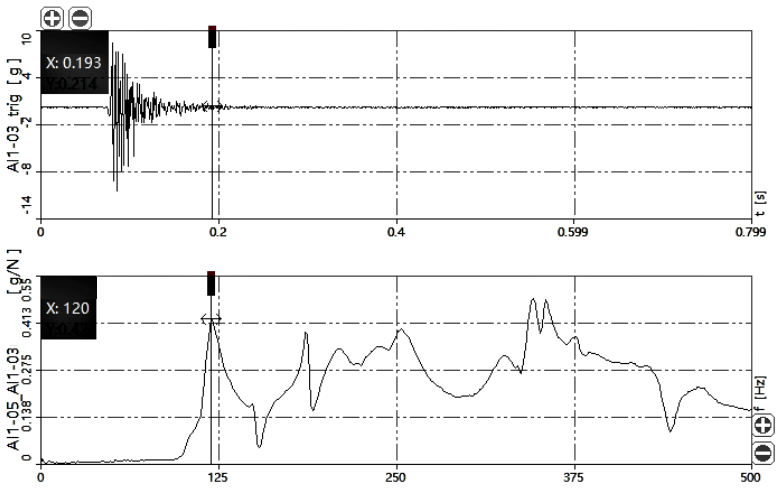

Figure 16: Tapping frequency response curve near measuring point 2

ISSN 2616-5767 Vol.7, Issue 5: 98-110, DOI: 10.25236/AJETS.2024.070513

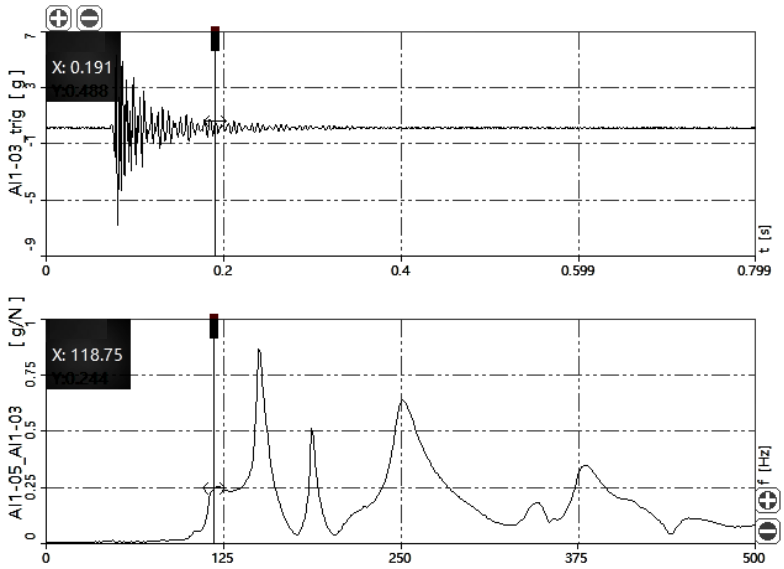

Figure 17: Frequency response curve of point 2 by randomly knock on the whole rudder plane

From the data curves, it can be observed that the first-order frequency of the rudder surface is approximately 118Hz, with an error of about 11.9% compared to the theoretical value of 132Hz. Considering the screw joint conditions of various components in the actual structure, as well as the influence of clearance between the pivot shaft and locking pin structure, the test results can verify the correctness of the theoretical model.

6. Conclusion

The research work in this paper addresses issues such as poor reliability of conventional circular spring pins and difficulties in ensuring locking performance. A spring square pin locking mechanism with self-locking inclined surfaces was designed and a comprehensive study on the locking performance was conducted. The main research findings are as follows:

1) On the basis of the design of the locking mechanism, a test prototype of a folding rudder was developed, and unfolding locking tests were carried out. The rudder surface can be effectively locked without any noticeable clearances at the mating surfaces, demonstrating that the spring square pin locking mechanism with self-locking inclined surfaces has a good locking effect.

2) A theoretical analysis model for the static stiffness in the locked state of the folding rudder was established, considering structural torsional stiffness, bending stiffness, and structural contact deformation. The evaluation of the overall stiffness was based on the maximum deformation displacement at the sagging point. Under the action of an equivalent concentrated force, the theoretical analysis showed an error of approximately 12.8% compared to simulation results. Concentrated force loading tests at the sagging point were conducted, showing an error below 15% compared to theoretical predictions. The accuracy of the theoretical model was validated by both simulation and experimental results.

3) A theoretical calculation model for the frequency characteristics in the locked state of the folding rudder was established, calculating the first-order bending and torsional modal frequencies of the folding rudder structure. Simulation analysis verified that the calculated natural frequencies of the structure were in good agreement with simulation results. Frequency tests using the impact method indicated a first-order frequency of approximately 118Hz for the rudder surface, with an error of about 11.9% compared to the theoretical value of 132Hz.

4) The research findings of this study can be applied to the design and theoretical verification analysis of folding rudder structures, facilitating improvements in rudder surface locking performance and significantly reducing the development cycle.

ISSN 2616-5767 Vol.7, Issue 5: 98-110, DOI: 10.25236/AJETS.2024.070513

References

[1] Kroyer, Robert. Wing mechanism analysis[J]. Computers & structures, 1999, 72(1/3): 253-265.
[2] Andrzej T, Tomasz G G.. Design of morphing wing with surface discontinuity[J]. Journal of Aerospace Engineering, 2018, 232(14): 2638-2650.
[3] Henry, J.L., Schwartz, D.R., Soukup, M., & Altman, A. Design, Construction, and Testing of a Folding-Wing[J]. Tube-Launched Micro Air Vehicle, 2005.
[4] Dowell EH., Tang D. Nonlinear aeroelasticity and unsteady aerodynamics[J]. AIAA journal, 2002, 40(9):1697-1707.
[5] Hu, Wei Yang, Zhichun Gu, Ying song. Aeroelastic study for folding wing during the morphing process [J]. Journal of Sound and Vibration, 2016: 365216-229.
[6] Hu, Wei Yang, Zhichun Gu, Ying song, et al. The nonlinear aeroelastic characteristics of a folding wing with cubic stiffness[J]. Journal of Sound and Vibration, 2017, 40022-39.
[7] Zhang,Wei, Lv, Shengli, Ni,Yingge. Parametric aeroelastic modeling based on component modal synthesis and stability analysis for horizontally folding wing with hinge joints[J]. Nonlinear dynamics, 2018, 92(2): 169-179.
[8] S.Bograd, P.Reuss, A.Schmidt, et al. Modeling the dynamics of mechanical joints[J]. Mechanical Systems & Signal Processing, 2011, 25(8): 2801-2826.
[9] Santos, Pedro D.R., Sousa, Diogo B., Gamboa, Penro V., et al. Effect of design parameters on the mass of a variable-span morphing wing based on finite element structural analysis and optimization[J]. Aerospace science and technology, 2018, 80(9):587-603.
[10] Abdelkefi A., Vasconcellos R., Marques F.D., et al. Modeling and identification of freeplay nonlinearity[J]. Journal of Sound and Vibration, 2012, 331(8): 1898-1907.
[11] M. V. Yarygina, Yu. I. Popov. Development of the weight formula for a folding wing [J]. Russian Aeronautics. 2012, 55(2):120-126.
[12] Dae-Kwan Kim,Jae-Sung Bae,In Lee. Dynamic Model Establishment of a Deployable Missile Control Fin with Nonlinear Hinge[J]. Journal of spacecraft and rockets. 2005, 42(1): 66-77.
[13] Jae-Sung Bae, Dae-Kwan Kim, Won-Ho Shin, et al. Nonlinear Aeroelastic Analysis of a Deployable Missile Control Fin[J]. Journal of spacecraft and rockets, 2004, 41(2): 264-271.